ACCOUNTS
of chemical research

Lanthanide-Doped Nanocrystals: Synthesis, Optical-Magnetic Properties, and Applications

GUOFENG WANG, QING PENG, AND YADONG LI*
Department of Chemistry, Tsinghua University, Beijing 100084, China

RECEIVED ON SEPTEMBER 26, 2010

CONSPECTUS

Because of the potential applications of lanthanide-doped nanocrystals in display devices, optical communication, solid-state lasers, catalysis, and biological labeling, the controlled synthesis of these new nanomaterials has sparked considerable interest. Nanosized phosphorescent or optoelectronic devices usually exhibit novel properties, depending on their structures, shapes, and sizes, such as tunable wavelengths, rapid responses, and high efficiencies. Thus, the development of facile synthetic methods towards high-quality lanthanide-doped nanocrystals with uniform size and shape appears to be of key importance both for the exploration of their materials properties and for potential applications.

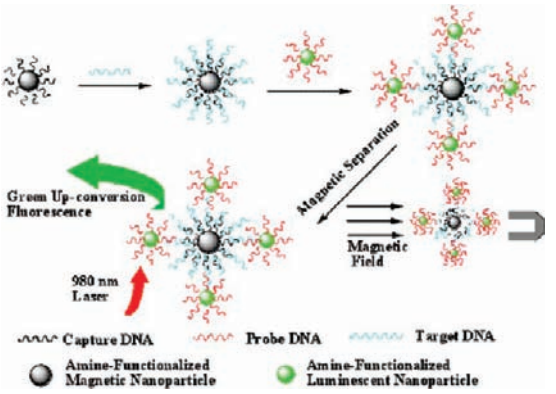

This Account focuses on the recent development in our laboratory of the synthesis and applications of lanthanide-doped nanocrystals. Since 2005, when we proposed a general strategy for nanocrystal synthesis via a liquid−solid−solution process, a range of monodisperse and colloidal lanthanide-doped fluoride, oxide, hydroxide, orthovanadate, thiooxide, borate, and phosphate nanocrystals have been successfully prepared. By rationally tuning the reaction conditions, we have readily synthesized nanostructures, such as hollow microspheres, nanorods, nanowires, hexagonal nanoplates, and nanobelts. By adjusting the different colloidal nanocrystal mixtures, we fabricated unique binary nanostructures with novel dual-mode luminescence properties through a facile ultrasonic method.

By tridoping with lanthanide ions that had different electronic structures, we successfully achieved β-$NaYF_4$ nanorods that were paramagnetic with tuned upconversion luminescence. We have also used $NaYF_4$:Yb^{3+}/Er^{3+} conbined with magnetite nanoparticles as a sensitive detection system for DNA: $NaYF_4$:Yb^{3+}/Er^{3+} and Fe_3O_4 nanoparticles were modified with two different DNA sequences. Then, the modified $NaYF_4$:Yb^{3+}/Er^{3+} nanoparticles were conjugated to the modified Fe_3O_4 nanoparticles. These binary nanoparticles can be hybridized with a third DNA (target DNA) molecule and separated with the assistance of a magnetic field. In addition, a novel fluorescence resonance energy transfer (FRET) method for nonenzymatic glucose determination has been developed by using the glucose-modified LaF_3:Ce^{3+}/Tb^{3+} nanocrystals. By using bioconjugated $NaYF_4$:Yb^{3+}/Er^{3+} nanoparticles as the energy donor and bioconjugated gold nanoparticles as the energy acceptor, we successfully developed a simple and sensitive fluorescence resonance energy transfer (FRET) biosensor for avidin. Meanwhile, we also carried out preliminary studies to investigate possible applications of lanthanide-doped nanocrystals in catalysis and in dye-sensitized solar cells.

1. Introduction

In recent years, great effort has been devoted to the controllable synthesis of rare earth (RE)-doped nanoparticles driven primarily by the fact that doped nanocrystalline phosphors yielded high luminescence efficiencies.[1] With rapidly shrinking size, nanomaterials display novel shape- and size-dependent properties for their extremely small size and relatively large specific surface areas.[2−6] Based on these unique properties, RE-doped nanocrystalline materials may play an outstanding role in display devices, optical telecommunication, solid-state lasers, and so on.[7] Therefore, the development of a facile synthetic method toward high-quality RE nanocrystals with uniform size and shape appears to be of key importance for the exploration of new research and application fields.[8−12]

RE-doped nanoparticles have been suggested as a promising new class of fluorescent probes. In comparison to organic dyes and semiconductor quantum dots, RE-doped

Published on the Web 03/11/2011 www.pubs.acs.org/accounts
10.1021/ar100129p

TABLE 1. The Crystal Structures, Morphologies, and Applications of Typical Ln-Doped Nanocrystals

samples		crystal structure	morphology	application
core@shell	$CeO_2@Ce_{1-x}Zr_xO_2$	cubic	hollow	catalysis
hydroxides	$Ln(OH)_3$, (Ln = Y, La, Pr, Nd, Sm, Eu, Gd, Dy, Tb, Ho, and Tm)	hexagonal	nanowires	
oxides	Ln_2O_3, (Ln = Y, La, Pr, Nd, Sm, Eu, Gd, Dy, Tb, Ho, and Tm)	cubic	nanowires	
	CeO_2		nanoflowers	
fluorides	$NaYF_4$:Ln^{3+} (Ln = Eu, Yb^{3+}, Ho^{3+}, Er^{3+}, Tm^{3+}, Gd^{3+}, and Ce^{3+})	hexagonal	nanorods	biology
		cubic	nanoparticles	
	LaF_3, CeF_3, PrF_3, and NdF_3	hexagonal	nanoparticles	
	SmF_3 and EuF_3		microparticles	
	GdF_3	orthorhombic	microparticles	
	YF_3		nanorices	
	CaF_2:Yb^{3+}/Er^{3+}	cubic	nanoparticles	
	BaF_2:Eu^{3+}	cubic	nanoparticles	
		orthorhombic	nanorods	
orthophosphate	$LaPO_4$	monoclinic	nanowires	lasers and biology
		hexagonal	nanorods	
	YPO_4	hexagonal	nanorods	
		tetragonal	nanoparticles	
	$CePO_4$	monoclinic	nanowires	
	$NdPO_4$		nanorods	
	$PrPO_4$, $EuPO_4$, and $TbPO_4$	hexagonal	nanorods	
	$SmPO_4$ and $GdPO_4$		nanowires	
	$DyPO_4$ and $LuPO_4$	tetragonal	nanoparticles	
orthovanadates	$LnVO_4$ (Ln = Y and lanthanides)	tetragonal	nanosheets	solar cells and biology

nanocrystals show superior chemical and optical properties, including low toxicity, large effective Stokes shifts, sharp emissions, long fluorescence lifetimes, and high resistance to photobleaching.[13−23] In addition, these nanoparticles can enable time-resolved fluorescence imaging for quantitative detection of antigens as well as tissue-specific transcripts and genes. More importantly, the RE nanoparticles have the potential to be used for noninvasive, nondestructive, and real-time in vivo diagnosis of various diseases, including atherosclerotic plaques, which can lead to stroke and heart disease.[24]

Multimodal bioimaging is a new frontier in biology and medicine, which combines more than one imaging modality, such as optical, ultrasound, nuclear, and magnetic resonance imaging (MRI).[25,26] It is well-known that Gd^{3+} complexes usually have paramagnetic properties at room temperature due to the $4f^7$ electronic configuration of Gd^{3+}. These paramagnetic Gd^{3+} complexes are widely used as contrast agents in MRI owing to their enhancement of the relaxation of the neighboring protons.[27] And thus, by codoping of Gd^{3+} and other RE ions in nanocrystals, a novel material possessing the advantages of fluorescent and magnetic properties could be achievable.[28]

Our interest in the chemistry of RE-doped nanocrystals started in the early 2000s, when we proposed a general strategy (liquid−solid−solution process) for nanocrystal synthesis.[29] Since then, a range of monodisperse and colloidal RE-doped fluoride, oxide, hydroxide, oxyhydroxide, orthovanadate, thiooxide, borate, and phosphate nanocrystals have been successfully prepared.[30−65] Subsequently, the applications of RE nanocrystals in biology, catalysis, and dye-sensitized solar cells were also studied preliminarily.[66−74]

In this Account, we summarize the progress that we have made over the past decade in the study of this unique class of RE-doped nanocrsytals. The crystal structure, morphology, and application of typical Ln-doped nanocrystals have been summarized in Table 1.

2. Synthetic Studies

2.1. Liquid−Solid−Solution (LSS) Process for the Synthesis of Monodisperse RE Fluorescent Nanocrystals. Over the past decade, monodisperse nanocrystals, which exhibit many interesting shape- and size-dependent phenomena and properties, have been extensively investigated for both their scientific and their technological applications.[29−45] Our group has reported a unified approach, the LSS process,[29] to the synthesis of a large variety of nearly monodisperse RE fluorescent nanocrystals with narrow size distribution (Figure 1). Detailed explanations of the LSS process can be found in ref 29. By tuning the synthetic conditions, such as dopant concentration, solvothermal temperature, and time, we have successfully prepared nanocrystals with different shapes. It is noted that the nanocrystals synthesized by the LSS process are hydrophobic. These hydrophobic nanocrystals could be further rendered hydrophilic by oxidizing oleic acid ligands on the surface of nanocrystals with Lemieux−von Rudloff reagent.[13]

2.2. Synthesis of 3D Colloidal Spheres. Using these dispersible RE nanocrystals mentioned above as building

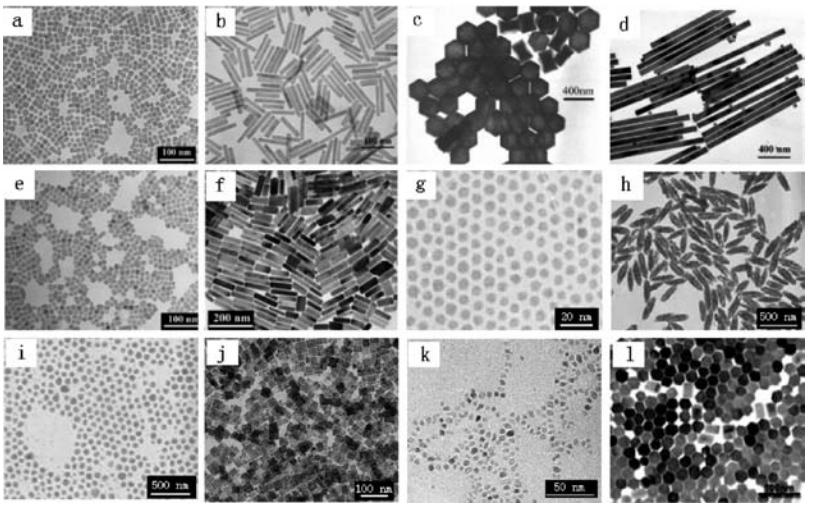

FIGURE 1. Typical TEM images of (a) $NaYF_4$:Tb, (b,c) $NaYF_4$:Eu, (d−f) $NaYF_4$:Yb−Er, (g) LaF_3, (h) YF_3, (i) YbF_3, (j) $LaVO_4$:Eu, (k) YBO_3:Eu, and (l) $YPO_4 \cdot 0.8H_2O$ nanocrystals.

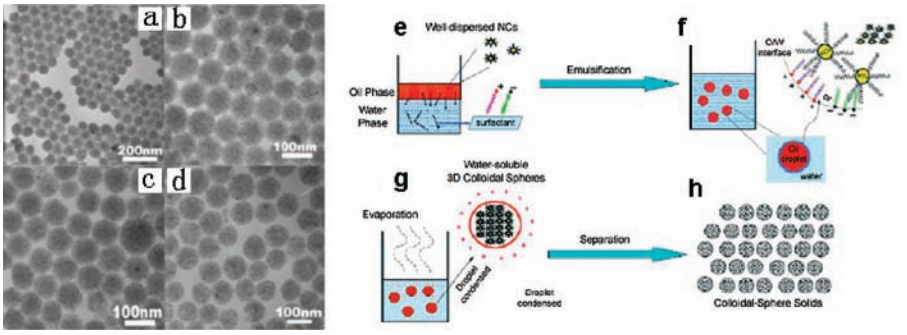

FIGURE 2. Typical TEM images of (a) LaF_3:Eu/LaF_3:Yb−Er, (b) $NaYF_4$:Tb/$NaYF_4$:Yb−Er, (c) LaF_3:Ce−Tb/$NaYF_4$:Yb−Er, and (d) LaF_3:Yb−Er. (e−h) Schematic of the EBS method: (e) mixture of oil phase and water phase (nanocrystals capped with ligands, well-dispersed in cyclohexane, are added to an aqueous solution of surfactant); (f) formation of the microemulsion system (oil droplets containing nanocrystals are stabilized by surfactant at the interface); (g) Evaporation of the low-boiling solvent in the oil droplets at a specified temperature, and the assembly process of the nanocrystals in the confined oil droplets into 3D colloidal spheres, which can be well-dispersed in water; (h) separation of the assembled 3D colloidal sphere solids from the solutions.

blocks, one can prepare 3D colloidal spheres by a simple microemulsion-based bottom-up self-assembly (EBS) method (Figure 2).[30,35] This method is based on a designed oil-in-water (O/W) microemulsion system. The nanocrystals are gathered, assembled, and fixed together spontaneously during controlled evaporation of a low-boiling oil solvent in the restricted, micrometer-sized 3D space provided by the microemulsion droplets. The composition, size, and surface charge of the colloidal spheres were controlled by rationally designing the experimental conditions.

2.3. Hydrothermal Synthesis of RE Compound Nanocrystals. Hydrothermal methods have been shown to be effective in the synthesis of nanowires, nanorods, and nanotubes.[47,51,59,63] Based on the preparation of RE hydroxide (or fluoride) colloidal precipitates at room temperature and the subsequent hydrothermal treatment at designated reaction conditions, a systematic study has been carried out to investigate the controlled formation of nanowires, nanosheets, and nanotubes.[51] Figure 3a−f shows the TEM images of lanthanide hydroxide nanowires and nanotubes.[47,51] Detailed reaction mechanisms of the hydrothermal method are provided in ref 47.

Recently, our group synthesized lanthanide hydroxide nanocrystals by regularly decomposing RE nitrates in octadecylamine (ODA).[65] The results indicate that the electron configuration, ionic radius, and crystal structure of lanthanide ions are responsible for the morphologies of the nanocrystals. For larger RE^{3+} ions (RE = La, Pr, Nd, Sm, Eu, and Gd), the lanthanide hydroxides exhibit plate-like nanostructures. For smaller RE^{3+} ions (RE = Y, Dy, Ho, Er, Tm, and Yb), the lanthanide hydroxides exhibit belt-like nanostructures. Tb^{3+} is a mid-sized RE^{3+} ion, and $Tb(OH)_3$ nanocrystals are rod-like. By calcination, the corresponding RE oxides with the same morphologies as their precursors were

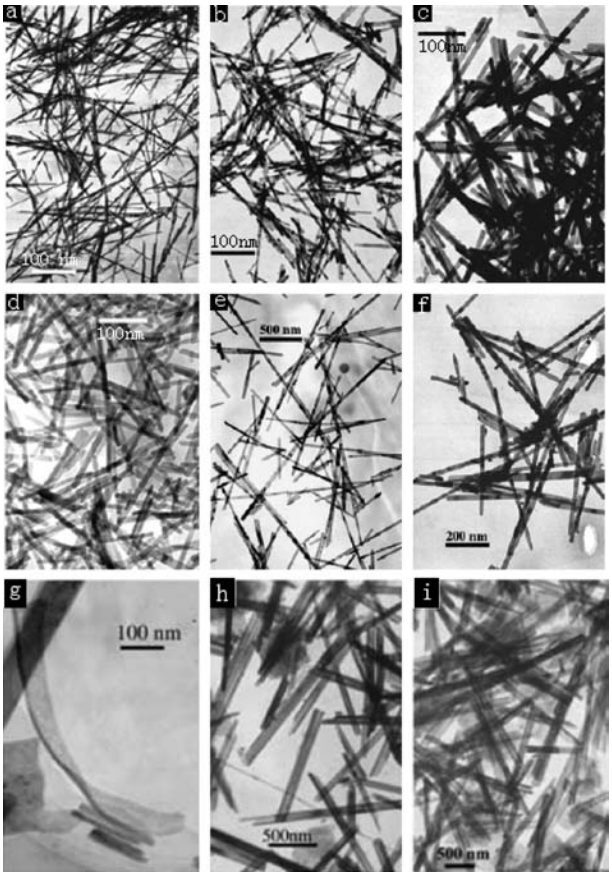

FIGURE 3. Typical TEM images of (a) $La(OH)_3$, (b) $Pr(OH)_3$, (c) $Eu(OH)_3$, (d) $Ho(OH)_3$, (e) $Sm(OH)_3$, and (f) $Gd(OH)_3$ nanowires, (g) $Er(OH)_3$ nanobelts, (h) $Yb(OH)_3$ nanotubes, and (i) $Tm(OH)_3$ nanotubes.

obtained. It is imperative to point out that flower-like cerium oxide could be obtained directly from the decomposition of the nitrate without further calcination.

3. Optical and Magnetic Property Studies

3.1. Tunable Upconversion (UC) Luminescence. Considerable interest has been centered on the frequency UC from infrared radiation to shorter wavelengths by using laser diodes as pump sources and RE materials as active emissive media.[6,7,10] In particular, the ability to manipulate UC color output opens the door to more complex, multiplexed labeling. Utilization of varied dopant−host combinations is one of the most straightforward approaches to obtain multicolor UC luminescence.[10]

We have taken $NaYF_4$:Yb^{3+}/Ho^{3+}/Ce^{3+} nanorods as an example to obtain the multicolor UC luminescence of RE-doped nanocrystals (Figure 4).[34] The results indicated that the relative intensity of $^5F_5 \rightarrow {}^5I_8$ to $^5S_2/^5F_4 \rightarrow {}^5I_8$ rises with increasing Ce^{3+} concentration, which can be attributed to the efficient energy transfers of $^5I_6$ (Ho) + $^2F_{5/2}$ (Ce) → $^5I_7$ (Ho) + $^2F_{7/2}$ (Ce) and $^5S_2/^5F_4$ (Ho) + $^2F_{5/2}$ (Ce) → $^5F_5$ (Ho) + $^2F_{7/2}$ (Ce). In addition, the $^5G_5 \rightarrow {}^5I_7$ and $^5F_2/^3K_8 \rightarrow {}^5I_8$ transitions of Ho^{3+} ions under infrared excitation were observed for the first time. With increasing Ce^{3+} concentration, the emission intensity of the $^5F_5-{}^5I_8$ gradually increased and that of the $^5S_2/^5F_4-{}^5I_8$ gradually decreased.

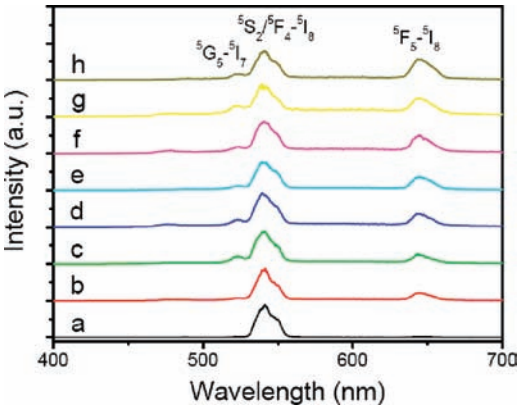

FIGURE 4. Dependence of UC luminescence spectra (normalized to $^5S_2/^5F_4 \rightarrow {}^5I_8$ transitions) on Ce^{3+} concentration (20% Yb^{3+} and 2% Ho^{3+}): (a) 0%; (b) 2%; (c) 3%; (d) 5%; (e) 10%; (f) 15%; (g) 20%; (h) 30%.

Another most important spectral feature of $NaYF_4$:Yb^{3+}/Ho^{3+}/Ce^{3+} nanorods is the dependence of UC luminescence upon the pump power (Figure 5). It is surprising to observe that the intensity ratio of $^5G_5 \rightarrow {}^5I_7$ to $^5S_2/^5F_4 \rightarrow {}^5I_8$ of $NaYF_4$:Yb^{3+}/Ho^{3+}/Ce^{3+} nanorods fluctuates with increasing pump power density. However, the luminescence of $NaYF_4$:Yb^{3+}/Ho^{3+} nanorods is always dominated by the $^5S_2/^5F_4 \rightarrow {}^5I_8$.

3.2. Dual-Mode Luminescnece from Hydrophilic RE Fluoride Colloidal Spheres. In order to advance the applications of RE nanocrystals in multiplexed and highly sensitive biossays, we fabricated hydrophilic dual-mode luminescent colloidal spheres that were composed of two distinct units, one offering down-converting luminescence under UV excitation and the other providing up-converting luminescence excited with a 980 nm laser.[35] Figure 6a shows the luminescence spectra of LaF_3:Eu/LaF_3:Yb−Er nanospheres. Under the excitation of 980 nm light, three emissions were observed, which are assigned to the $^2H_{1/2} \rightarrow {}^4I_{5/2}$, $^4S_{3/2} \rightarrow {}^4I_{5/2}$, and $^4F_{9/2} \rightarrow {}^4I_{5/2}$ transitions of Er^{3+} ions. When excited at 396 nm, the $^5D_0 \rightarrow {}^7F_1$ and $^5D_0 \rightarrow {}^7F_2$ transitions of Eu^{3+} were observed.

Figure 6b−d shows the luminescence spectra of $NaYF_4$:Tb/$NaYF_4$:Yb−Er, LaF_3:Ce−Tb/$NaYF_4$:Yb−Er, and LaF_3:Ce−Tb/LaF_3:Yb−Er nanospheres. Similar to LaF_3:Eu/LaF_3:Yb−Er nanospheres, under 980 nm excitation, the emissions of Er^{3+} were observed. Under UV excitation, there are four emission peaks of Tb^{3+} at ∼489, ∼543, ∼587, and

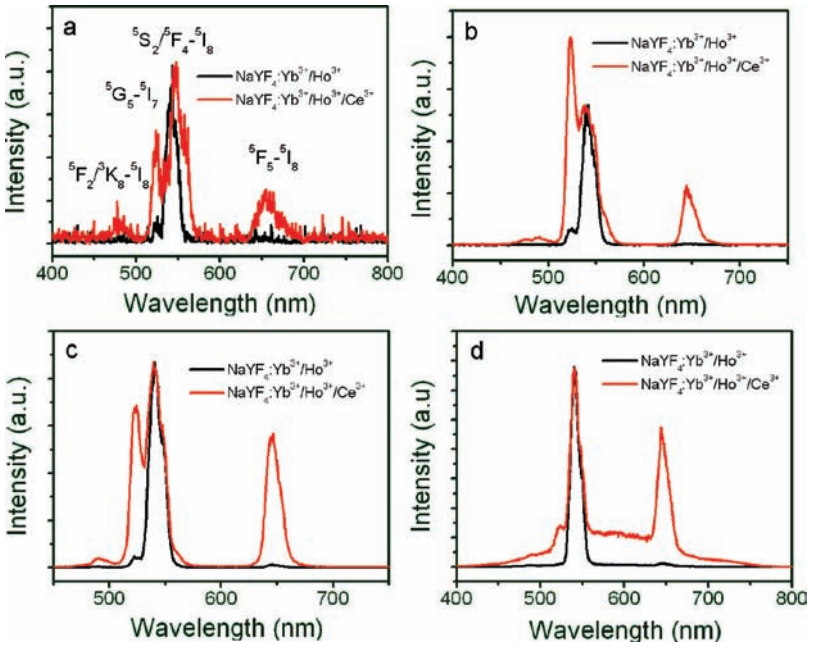

FIGURE 5. UC luminescence spectra of $NaYF_4:Yb^{3+}/Ho^{3+}$(20/2) and $NaYF_4:Yb^{3+}/Ho^{3+}/Ce^{3+}$(20/2/30) nanorods under different excitation power density: (a) 140; (b) 300; (c) 450; (d) 680 W/cm^2.

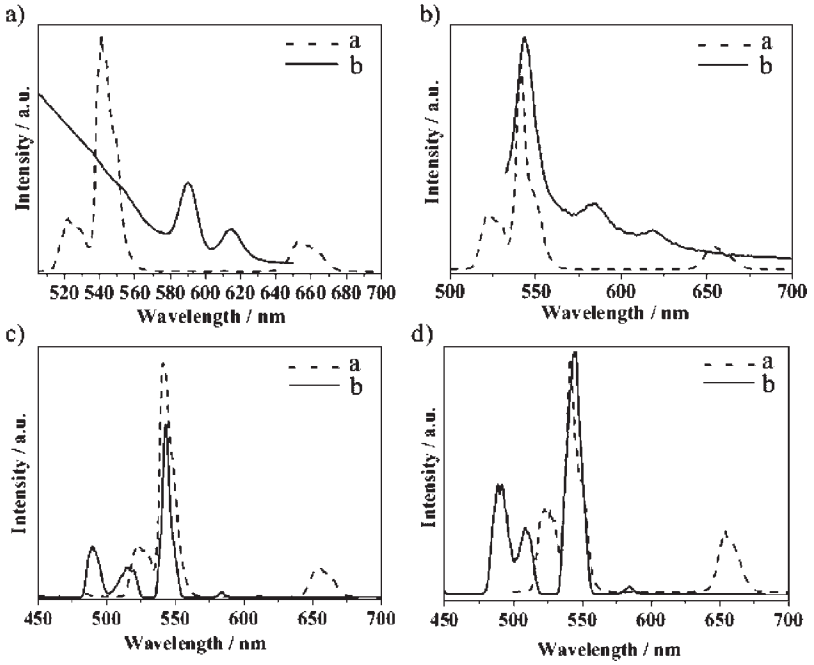

FIGURE 6. Down- and up-converting luminescence spectra of the as-obtained nanospheres: (a) LaF_3:Eu/LaF_3:Yb−Er; (b) $NaYF_4$:Tb/$NaYF_4$:Yb−Er; (c) LaF_3:Ce−Tb/$NaYF_4$:Yb−Er; (d) LaF_3:Ce−Tb/LaF_3:Yb−Er (−−−, a, downconverting luminescence spectra; —, b, upconverting luminescence spectra).

~618 nm, attributed to the $^5D_4 \rightarrow {}^7F_6$, $^5D_4 \rightarrow {}^7F_5$, $^5D_4 \rightarrow {}^7F_4$, and $^5D_4 \rightarrow {}^7F_3$ transitions, respectively. This strategy may provide new routes to rationally assemble nanometer-scale building blocks into multifunctional superstructures.

3.3. Bifunctional Optical−Magnetic Nanorods: β-$NaYF_4:Ln^{3+}$. As mentioned above, optical and magnetic materials have attracted much attention due to their importance in the fields of chemistry, biology, medical sciences, and biotechnology. We successfully prepared bifunctional β-$NaYF_4:Ln^{3+}$ (Ln = Yb/Gd/Tm and Yb/Gd/Er) nanorods according to our reported LSS strategy.[34] The obtained nanorods not only can exhibit paramagnetic behavior at room

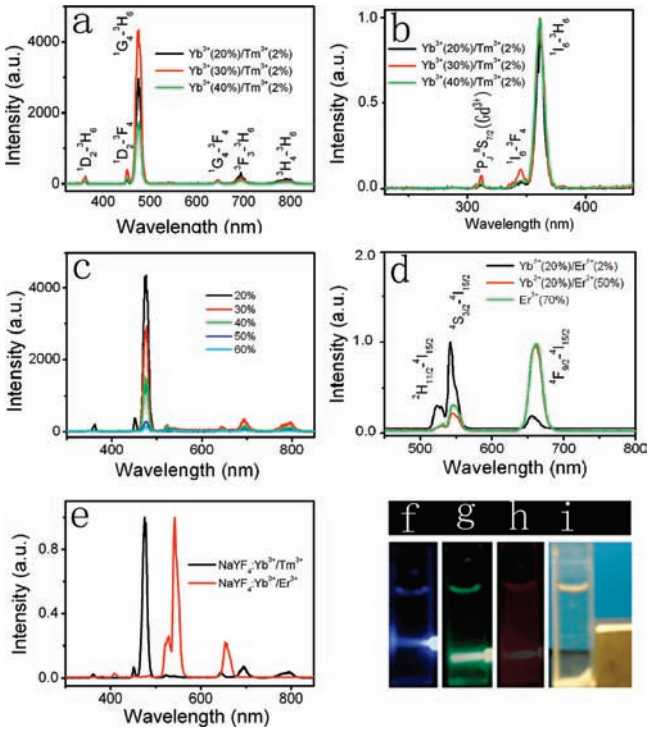

FIGURE 7. UC luminescence spectra of (a,b) $NaYF_4$:Yb^{3+}/Gd^{3+}/Tm^{3+} (x/30/2), (c) $NaYF_4$:Yb^{3+}/Gd^{3+}/Tm^{3+} (30/x/2), and (d) $NaYF_4$:Yb^{3+}/Gd^{3+}/Er^{3+} (x/20/x) nanorods in cyclohexane. For comparison, the UC luminescence spectra of $NaYF_4$:Yb^{3+}/Tm^{3+} and $NaYF_4$:Yb^{3+}/Er^{3+} nanorods are also shown panel e. Compiled luminescent photos showing corresponding colloidal solutions of (f) $NaYF_4$:Yb^{3+}/Gd^{3+}/Tm^{3+}(30/20/2), (g) $NaYF_4$:Yb^{3+}/Gd^{3+}/Er^{3+}(30/20/2), and (h) $NaYF_4$:Gd^{3+}/Er^{3+}(20/70). (i) The photo of $NaYF_4$:Yb^{3+}/Gd^{3+}/Tm^{3+} colloidal solution in the presence of a magnet.

temperature but also can emit fine-tuning UC emissions spanning from the UV to the near-infrared under 980 nm excitation.

The UC luminescent sprectra of $NaYF_4$:Yb^{3+}/Gd^{3+}/Tm^{3+}-(Er^{3+}) nanorods are shown in Figure 7. Upon excitation at 980 nm, the $NaYF_4$ nanorods doped with Yb/Gd/Tm exhibit characteristic sharp emission peaks, which can be attributed to the $^6P_{5/2} \rightarrow {}^8S_{7/2}$ and $^6P_{7/2} \rightarrow {}^8S_{7/2}$ transitions of Gd^{3+} and the $^1I_6 \rightarrow {}^3F_4$, $^1D_2 \rightarrow {}^3H_6$, $^1D_2 \rightarrow {}^3F_4$, $^1G_4 \rightarrow {}^3H_6$, $^1G_4 \rightarrow {}^3F_4$, $^3F_3 \rightarrow {}^3H_6$, and $^3H_4 \rightarrow {}^3H_6$ transitions of Tm^{3+}. The optimum concentrations of Yb^{3+} and Gd^{3+} ions are 30% and 20%, respectively. Here, the Ln^{3+} concentrations refer to the initial dopant concentrations of reactants. The UC emission spectra of $NaYF_4$:Yb^{3+}/Gd^{3+}/Er^{3+} nanorods are shown in Figure 7d. These emission peaks can be attributed to the $^2H_{11/2} \rightarrow {}^4I_{15/2}$, $^4S_{3/2} \rightarrow {}^4I_{15/2}$, and $^4F_{9/2} \rightarrow {}^4I_{15/2}$ transitions of Er^{3+} ions. It is noted that upon doping with increased concentrations of Yb^{3+} and Er^{3+}, one can precisely manipulate the relative emission intensities of the two constituent

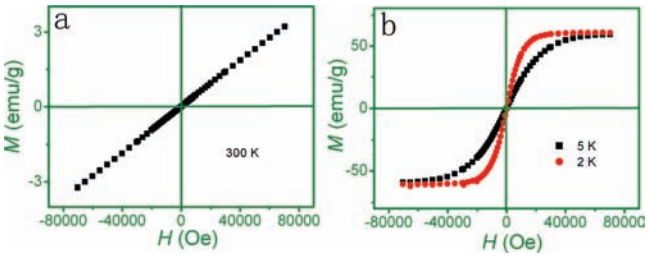

FIGURE 8. Magnetization curves of $NaYF_4$:Yb^{3+}/Gd^{3+}/Tm^{3+} nanorods.

colors, thus resulting in tunable color output of the nanorods from green to red.

Apart from the aforementioned luminescence properties, the $NaYF_4$:Yb^{3+}(30%)/Gd^{3+}(40%)/Tm^{3+}(2%) nanorods are paramagnetic at room temperature (Figure 8). At 2 or 5 K, the nanorods are superparamagnetic with saturation magnetization value of about 60 emu g^{-1}. It is well-known that the magnetic behavior is highly size dependent. When the size of the ferromagnetic particles is reduced to a critical value, the magnetic property is no longer ferromagnetic but superparamagnetic. Usually, Gd^{3+} complexes have paramagnetic properties beyond magnetic ordering temperature and exhibit magnetic order below the magnetic ordering temperature. In this work, the average diameter of nanorods is ~50 nm, and thus, it is not surprising to observe that $NaYF_4$:Yb^{3+}/Gd^{3+}/Tm^{3+} nanorods are superparamagnetic at 2 or 5 K. These UC luminescent and paramagnetic properties of the nanorods underscore their potential as robust UC luminescence and magnetic resonance dual-mode fluorescent labels for bioimaging applications. It is noted that the magnetic susceptibility of $NaYF_4$:Yb^{3+}/Gd^{3+}/Tm^{3+} increased with increasing Gd^{3+} concentration.

3.4. Tunable Magnetic Properties of Magnetite by RE Doping. Nanometer-sized iron oxides and oxyhydroxide compounds are of great industrial and scientific importance. For example, nanoparticular magnetite has been widely applied in catalysis, energy storage, magnetic data storage, and ferrofluids for its unique electric and magnetic properties. Doped iron oxides, especially the spinel-structured MFe_2O_4, have shown tunable magnetic properties and attracted research interest for magnetic storage and catalysis.[67]

Five kinds of RE ions (Gd, Sm, Nd, Y, and Lu) were selected to be doped into magnetite to investigate the influence of RE doping on the magnetic properties of magnetite.[67] Here, the concentrations of the RE ions are 50%. The results indicate that lanthanide ions have a great effect on the magnetic properties of magnetite (Figure 9e–i). For comparison, the magnetization curves of undoped magnetite nanoparticles with different sizes are shown in Figure 9a–d. Magnetite

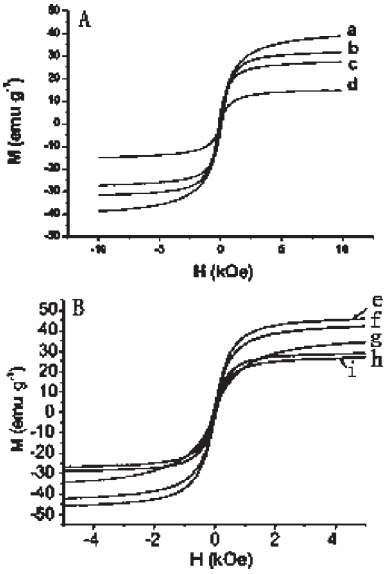

FIGURE 9. (A) Magnetization curves for undoped magnetite nanoparticles with different sizes: (a) 15.8, (b) 14.5, (c) 6.4, and (d) 4.7 nm. (B) Magnetization curves for magnetite doped with different kinds of lanthanides: (e) Gd, (f) Sm, (g) Lu, (h) Y, and (i) Nd.

samples doped with Gd^{3+} have the highest saturation magnetization of 45.9 emu g^{-1}. In contrast, the sample doped with Nd^{3+} has the smallest saturation magnetization of 26.8 emu g^{-1}. It can also be seen from the magnetization curves that the powders doped with Sm, Lu, and Gd are superparamagnetic with zero coercivity in contrast to the samples doped with Nd and Y, which exhibit a small hysteresis loop.

4. Application Exploration

4.1. Biological Applications. Optical and magnetic materials have attracted much attention due to their importance in the fields of chemistry, biology, medical sciences, and biotechnology. By combination of magnetic-field-assisted biochemical separation and concentration technology, novel composite materials of Fe_3O_4 and $NaYF_4$:Yb^{3+}/Er^{3+} have been applied to the sensitive detection of DNA (Figure 10).[69] The luminescent nanoparticles we chose were water-soluble $NaYF_4$:Yb^{3+}/Er^{3+} with a mean size of about 50 nm. Under 980 nm excitation, these nanoparticles can emit strong green UC fluorescence. The magnetic nanoparticles applied here were Fe_3O_4. These magnetic nanoparticles have an average size of about 150 nm with a smooth surface. The measurements of magnetic properties reveal that these magnetite nanoparticles have excellent saturation magnetization up to 83.1 emu g^{-1}.

Both the magnetic and luminescent nanoparticles were functionalized with polyelectrolyte using layer-by-layer (LbL) technology to introduce an amino group that could be

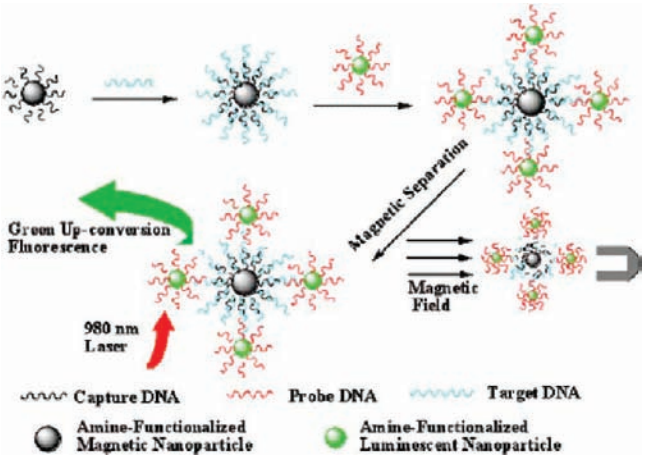

FIGURE 10. Scheme of the DNA assay method combining UC fluorescence with magnetic separation.

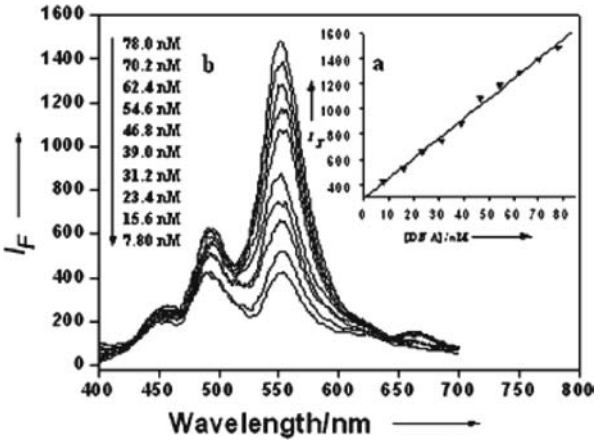

FIGURE 11. Fluorescence spectra of binary nanocomposite in the presence of different concentrations of target DNA (b) and the linear relationship (a) between luminescence intensity and target DNA content according to panel b.

attached to nucleic acids (Figure 10). In a typical experiment for DNA detection, magnetic nanoparticles were modified with capture DNA (39-AAT-TGA-GGA-GAA-AGA-A_{10}-$(CH_2)_3$-SH) and phosphor nanoparticles were modified with probe DNA (59-TCC-ATG-CAA-CTC-TAA-A_{10}-$(CH_2)_3$-SH), respectively. These capture DNA modified magnetite nanoparticles can be hybridized with target DNA (59-TTA-GAG-TTG-CAT-GGA-TTA-ACT-CCT-CTT-TCT-39) and separated with an assistant magnetic field. Then, the probe DNA modified luminescent nanoparticles were conjugated to the magnetic nanoparticles through the hybridization with the overhanging region of the target sequences. The binary nanoparticles were purified with magnetic separation and detected with UC fluorescence technology. As shown in Figure 11, the concentration of the target DNA in the range

of 7.8—78.0 nM is linear to the UC luminescence intensities. The linear calibration equation, $F_{UC} = 292.4 + 15.7C$ of the detection was obtained according to the general detection procedure. F_{UC} and C represented the intensity of luminescence and the concentration of the target DNA, respectively.

In addition, by use of bioconjugated $NaYF_4:Yb^{3+}/Er^{3+}$ nanoparticles as energy donor and bioconjugated gold nanoparticles as energy acceptor, a simple and sensitive fluorescence resonance energy transfer (FRET) biosensor for avidin has been successfully developed.[68] Based on FRET between nonenzymatic glucose modified $LaF_3:Ce^{3+}/Tb^{3+}$ nanocrystals and the 3-aminophenylboronic acid modified rhodamine B isothiocyanate, we have also demonstrated a novel biosensor for the detection of glcose.

4.2. Catalytic Applications. Nanosized RE compounds present great promise and opportunities for a new generation of catalysts. It is known that the reactivity depends on the crystal plane of the catalyst for structure-sensitive reactions.[72,76−78] Therefore, a desirable goal for catalyst design and synthesis would be to decrease the area of the less reactive crystal planes and increase that of the more reactive ones so as to optimize the desired structure of the active sites. Shape-controlled synthesis of nanostructured materials may present an opportunity for the synthesis of catalytic materials with such desirable features because these novel materials nucleate and grow in an epitaxial manner, exposing defined crystal planes.

Here, we take CeO_2 as an example to study the crystal plane effect of RE nanocrystals in catalysis application.[72] There are three low-index planes in the ceria fluorite cubic structure, namely, the very stable and neutral {111} plane, the less stable {110} plane, and the higher-energy {001} plane. Yang et al. have found that there are different adsorption features for CO on {111} and {110} planes. There are only weak adsorptions on the {111} plane,[75] whereas both weak and strong adsorptions are found on the {110} plane. If exposed planes with higher surface energy could be generated and stabilized, they could provide active sites for catalytic reactions.

CeO_2 nanorods and nanoparticles were synthesized via a hydrothermal method and a direct precipitation method, respectively. The HRTEM results reveal that CeO_2 nanorods predominantly expose the well-defined and less stable {001} and {110} planes, whereas in the CeO_2 nanoparticles, the most stable {111} planes are predominantly exposed. Measurements were made of the catalytic activity of CO oxidation (Figure 12). Obviously, CeO_2 nanorods were more active than CeO_2 nanoparticles. At 190 °C, the percentage CO conversion was 40% over the CeO_2 nanorods and only 17% over the nanoparticles. The rate of conversion of CO over CeO_2 nanorods was three times higher than that over nanoparticles.

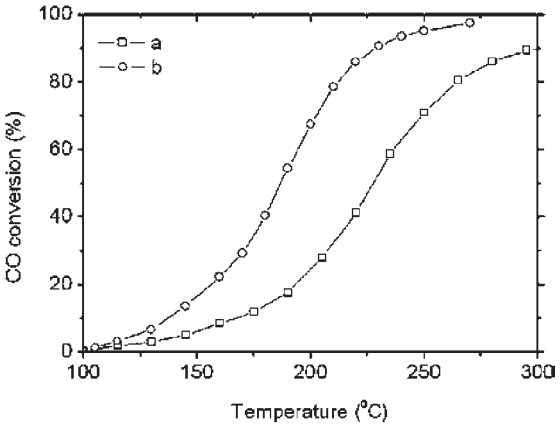

FIGURE 12. Percentage conversion versus temperature plots for the oxidation of CO over (a) CeO_2 nanoparticles and (b) CeO_2 nanorods.

In general, high-surface-area nanocatalytic materials exhibiting numerous crystal faces, edges, and corners, which are conventionally considered active sites for the adsorption of reactants, should generate better catalytic performance. However, CeO_2 nanoparticles, with higher surface area and smaller particle size, were poorer catalysts, whereas CeO_2 nanorods, with lower surface area and larger diameter, were more active and demonstrated a stable redox property. These unusual results for these two ceria nanomaterials inspire us to hope that specific crystal planes are indeed a determining factor that will prove useful. Similar phenomena were observed in the study on the catalytic performance of CuO and Ag nanocrystals with different shapes.

Recently, our group selected Er_2O_3 nanobelts as catalyst supports and investigated the catalytic activity of Au-nanoparticle-deposited Er_2O_3 nanocatalysts for CO oxidation. Although Er_2O_3 nanobelts might not be the most excellent support in the case of Au-supported catalysts for CO oxidation, the experiment indicates their potential applications as catalysts or catalyst supports for other important reactions such as selective oxidation of ethane to ethylene.

4.3. The Application of RE Nanocrystals in Dye-Sensitized Solar Cells. Dye-sensitized solar cells (DSSCs) have been investigated intensively as a cost-effective alternative to conventional solar calls.[70] In DSSCs, TiO_2 films have been widely used as the photoanode onto which dye sensitizers were adsorbed. Some researchers have reported that the photoanodes prepared from organized mesoporous TiO_2 films showed enhanced solar-cell conversion efficiency

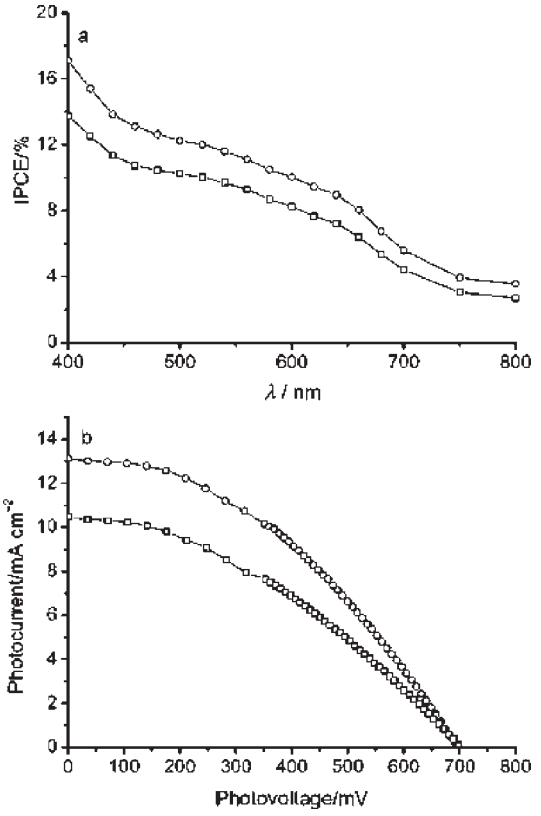

FIGURE 13. (a) Action spectra and (b) current−voltage cures of DSSCs: (○) = modified; (□) = unmodified.

relative to that of traditional films of the same thickness made from randomly oriented anatase nanocrytals. Therefore, replacing the nanoparticle film with an array of oriented single-crystalline nanowires was investigated. Unfortunately, the efficiency was limited because of the small surface area of the nanowires. Therefore, it is important to modify the titania electrodes for enhancing solar-cell conversion efficiency.

RE ions have unique electronic structures and numerous transition modes, and thus, by introducing RE ions into the photoanode of the DSSCs, some novel properties can be expected. Monodisperse Nd-doped TiO_2 nanorods (20 nm × 2 nm) were synthesized by a solvothermal method.[67] These nanorods were easily embedded into the TiO_2 electrode in DSSCs and did not affect the adsorption amount of dye sensitizer. The result indicates that this incorporation of Nd-doped TiO_2 nanorods into TiO_2 electrode remarkably enhanced the short-circuit photocurrent and the fill factor, thus leading to a 33.3% increase in power conversion efficiency (Figure 13).[67] The mechanism is likely to be that Nd ions doped on TiO_2 nanorods to enhance the injection of excited electrons and decrease the recombination rate of the injected electrons. The introduction of rods not only decreases the total series resistance of a cell but also accelerates the transport rate of the injected electrons, consequentially improving the collection rate of injected electrons. The incorporation of Nd-doped TiO_2 nanorods into randomly assembled mesoporous films is a novel strategy to modify the photoanode in DSSCs.

We also prepared transparent Dy^{3+}-doped $LaVO_4$ film, which was used to coat solar cells. By combination of Dy-doped $LaVO_4$ luminescent film onto the back of the solar cell, the lifetime of the solar cell was greatly enhanced.[66] Especially, the downconverted light can be reabsorbed by solar cell and generate currentl hence the solar cell with the luminescent film improved energy conversion efficiency by 23.3% relative to the referenced one coated with an undoped $LaVO_4$ film.

5. Conclusion and Perspectives

This Account summarizes our recent progress on the synthesis, properties, and applications of lanthanide-doped nanocrystals. The growing interest in these doped nanomaterials is primarily due to the interesting structure-, shape-, and size-dependent properties, allowing their use in display devices, optical communication, solid-state lasers, catalysis, biological assays, and medical imaging. Because research on lanthanide-doped nanocrystals is still in its infancy, many of the materials properties and potential uses are yet to be discovered.

It is noted that there are a number of challenges ahead in the path toward practical applications of lanthanide-doped nanocrystals. For example, the luminescent efficiency, water solubility, biologic compatibility, stability, multicolor, and multifunction of nanocrystals are still the most influential factors for the practically biological application that deserve intense research attention, which is not only influenced by the electronic structure and concentration of doping RE ions but also influenced by the structure, shape, size, and synthetic method of nanocrystals. Although great strides have been made in these areas, future advances in controllable synthesis of lanthanide-doped nanocrystals with improved properties are essential before these promises are fulfilled. Our dream is to understand the formation mechanism at the molecular level by chemically controlling the formation process of lanthanide-doped nanocrystals and eventually to replace the empirical strategy by *ab initio* design. Meanwhile, integration of monodisperse lanthanide-doped nanocrystals into complex devices or superstructures is another goal of researchers in nanoscience fields.

We are grateful to all our co-workers, whose names are cited in the references, for their valuable contributions to this work.

We also thank the State Key Project of Fundamental Research for Nanoscience and Nanotechnology (Grant 2011CB932401), the Foundation for Innovative Research Groups of the National Natural Science Foundation of China (Grant 20921001), and the National Natural Science Foundation of China (Grant 10979032).

BIOGRAPHICAL INFORMATION

Guofeng Wang received her M.S. degree in Physics from Northeast Normal University in 2005 and Ph.D. degree in Electronic Science and Engineering from Jilin University in 2008. She joined the research group of Professor Yadong Li as a postdoctoral associate in 2009.

Qing Peng received his B.S. degree in Chemistry from Peking University in 1992 and Ph.D. degree in Chemistry from Tsinghua University in 2003, under the direction of Professor Yadong Li. He joined the faculty of the Department of Chemistry, Tsinghua University, in 2003 and was promoted to associate professor in 2006.

Yadong Li received his B.S. degree in Chemistry from Anhui Normal University in 1986 and Ph.D. degree in Chemistry from the University of Science and Technology of China in 1998, under the direction of Professor Yitai Qian. He joined the faculty of the Department of Chemistry, Tsinghua University, in 1999 as a full professor.

FOOTNOTES

*E-mail: ydli@mail.tsinghua.edu.cn.

REFERENCES

1 Bhargava, R.; Gallaghar, D.; Hong, X.; Nurmikko, A. Optical Properties of Manganese-Doped Nanocrystals of ZnS. *Phys. Rev. Lett.* **1994**, *72*, 416–419.

2 Boyer, J.; Vetrone, F.; Cuccia, L.; Capobianco, J. Synthesis of Colloidal Upconverting $NaYF_4$ Nanocrystals Doped with Er^{3+}, Yb^{3+} and Tm^{3+}, Yb^{3+} via Thermal Decomposition of Lanthanide Trifluoroacetate Precursors. *J. Am. Chem. Soc.* **2006**, *128*, 7444–7445.

3 Lehmann, O.; Kömpe, K.; Haase, M. Synthesis of Eu^{3+}-Doped Core and Core/Shell Nanoparticles and Direct Spectroscopic Identification of Dopant Sites at the Surface and in the Interior of the Particles. *J. Am. Chem. Soc.* **2004**, *126*, 14935–14942.

4 Heer, S.; Kömpe, K.; Güdel, H.; Haase, M. Highly Efficient Multicolour Upconversion Emission in Transparent Colloids of Lanthnide-Doped $NaYF_4$ Nanocrystals. *Adv. Mater.* **2004**, *16*, 23–24.

5 Mai, H.; Zhang, Y.; Yan, Z.; Sun, L.; You, L.; Yan, C. High-Quality Sodium Rare-Earth Fluoride Nanocrytals: Controlled Synthesis and Optical Properties. *J. Am. Chem. Soc.* **2006**, *128*, 6426–6436.

6 Wang, F.; Liu, X. Recent Advances in the Chemistry of Lanthanide-Doped Upconversion Nanocrystals. *Chem. Soc. Rev.* **2009**, *38*, 976–989.

7 Qin, G.; Qin, W.; Wu, C.; Huang, S.; Zhang, J.; Lu, S.; Zhao, D.; Liu, H. Enhancement of Ultraviolet Upconversion in Yb^{3+} and Tm^{3+} Codoped Amorphous Fluoride Film Prepared by Pulsed Laser Deposition. *J. Appl. Phys.* **2003**, *93*, 4328–4330.

8 Zijlmans, H.; Bonnet, J.; Burton, J.; Kardos, K.; Vail, T.; Niedbala, R.; Tanke, H. Detection of Cell and Tissue Surface Antigens Using Up-Converting Phosphors: A New Reporter Technology. *Anal. Biochem.* **1999**, *267*, 30–36.

9 Qin, W.; Zhang, D.; Zhao, D.; Wang, L.; Zheng, K. Near-Infrared Photocatalysis Based on YF_3:Yb^{3+},Tm^{3+}/TiO_2 core/shell Nanoparticles. *Chem. Commun.* **2010**, *46*, 2304–2306.

10 Rijke, F.; Zijlmans, H.; Li, S.; Vail, T.; Raap, A.; Niedala, R.; Tanke, H. Up-converting phosphor reporters for nucleic acid microarrays. *Nat. Biotechnol.* **2001**, *19*, 273–276.

11 Lim, S.; Riehn, R.; Ryu, W.; Khanarian, N.; Tung, C.; Tank, D.; Austin, R. In Vivo and Scanning Electron Microscopy Imaging of Upconverting Nanophosphors in Caenorhabditis elegans. *Nano Lett.* **2006**, *6*, 169–174.

12 Chen, Z.; Chen, H.; Hu, H.; Yu, M.; Li, F.; Zhang, Q.; Zhou, Z.; Yi, T.; Huang, C. Versatile Synthesis Strategy for Carboxylic Acid-functionalized Upconverting Nanophosphors as Biological Labels. *J. Am. Chem. Soc.* **2008**, *130*, 3023–3029.

13 Mahalingam, V.; Vetrone, F.; Naccache, R.; Speghini, A.; Capobianco, A. Colloidal Tm^{3+}/Yb^{3+} Doped $LiYF_4$ Nanocrystals: Multiple Luminescence Spanning the UV to NIR Regions via Low-Energy Excitation. *Adv. Mater.* **2009**, *21*, 1–4.

14 Wang, F.; Xue, X.; Liu, X. Multicolor Tuning of (Ln, P)-Doped YVO_4 Nanoparticles by Single-Wavelength Excitation. *Angew. Chem., Int. Ed.* **2008**, *47*, 906–909.

15 Li, C.; Yang, J.; Quan, Z.; Yang, P.; Kong, D.; Lin, J. Different Microstructures of β-$NaYF_4$ Fabricated by Hydrothermal Process: Effects of pH Values and Fluoride Sources. *Chem. Mater.* **2007**, *19*, 4933–4942.

16 Bai, X.; Song, H.; Pan, G.; Lei, Y.; Wang, T.; Ren, X.; Lu, S.; Dong, B.; Dai, Q.; Fan, L. Size-Dependent Upconversion Luminescence in Er^{3+}/Yb^{3+}-Codoped Nanocrystalline Yttria: Saturation and Thermal Effects. *J. Phys. Chem. C* **2007**, *111*, 13611–13617.

17 Yi, G.; Chow, G. Water-Soluble $NaYF_4$:Yb,Er(Tm)/$NaYF_4$/Polymer Core/Shell/Shell Nanoparticles with Significant Enhancement of Upconversion Fluorescence. *Chem. Mater.* **2007**, *19*, 341–343.

18 Charina, C. L.; Koski, K. J.; Olson, A. C. K.; Alivisatos, A. P. Luminescent Nanocrystal Stress Gauge. *Proc. Natl. Acad. Sci. U.S.A.* **2010**, *107*, 21306–21310.

19 Schrier, J.; Demchenko, D. O.; Wang, L. W.; Alivisatos, A. P. Optical Properties of ZnO/ZnS and ZnO/ZnTe Heterostructures for Photovoltaic Applications. *Nano Lett.* **2007**, *7*, 2377–2382.

20 Park, H. C.; Barrelet, C. J.; Wu, Y.; Tian, B.; Qian, F.; Lieber, C. M. A Wavelength-Selective Photonic-Crystal Waveguide Coupled to a Nanowire Light Source. *Nat. Photonics* **2008**, *2*, 622–626.

21 Chen, K. M.; Mirkin, C. A.; Lo, R. K.; Zhao, J.; McDevitt, J. T. Surveying the Surface Coordination Chemistry of a Superconductor: Spontaneous Adsorption of Monolayer Films of Redox-Active Ligands on $YBa_2Cu_3O_{7-d}$. *J. Am. Chem. Soc.* **1995**, *117*, 6374–6375.

22 Gao, X.; Nie, S. Quantum Dot-Encoded Beads. *Methods Mol. Biol.* **2005**, *303*, 61–71.

23 Yan, H.; He, R.; Johnson, J.; Law, M.; Saykally, R.; Yang, P. Dendrite Nanowire UV Laser Array. *J. Am. Chem. Soc.* **2003**, *125*, 4728–4729.

24 Dosev, D.; Nichkova, M.; Liu, M.; Guo, G.; Hammock, B.; Kenedy, I. Application of Luminescent Eu:Gd_2O_3 Nanoparticles to the Visualization of Protein Micropatterns. *J. Biomed. Opt.* **2005**, *10*, No. 064006.

25 Zhang, M.; Shi, S.; Meng, J.; Wang, X.; Fan, H.; Zhu, Y.; Wang, X.; Qian, Y. Preparation and Characterization of Near-Infrared Luminescent Bifunctional Core/Shell Nanocomposites. *J. Phys. Chem. C* **2008**, *112*, 2825–2830.

26 Cheon, J.; Lee, J. Synergistically Integrated Nanoparticles as Multimodal Probes for Nanobiotechnology. *Acc. Chem. Res.* **2008**, *41*, 1630–1640.

27 Hüber, M.; Staubli, A.; Kustedjo, K.; Gray, M.; Shih, J.; Fraser, S.; Jacobs, R.; Meade, T. Fluorescently Detectable Magnetic Resonance Imaging Agents. *Bioconjugate Chem.* **1998**, *9*, 242–249.

28 Kumar, R.; Nγk, M.; Ohulchansk$\gamma\gamma$, T.; Flask, C.; Prasad, P. Combined Optical and MR Bioimaging Using Rare Earth Ion Doped $NaYF_4$ Nanocrystals. *Adv. Funct. Mater.* **2009**, *19*, 853–859.

29 Wang, X.; Zhuang, J.; Peng, Q.; Li, Y. A General Strategy for Nanocrystal Synthesis. *Nature* **2005**, *437*, 121–124.

30 Bai, F.; Wang, D.; Huo, Z.; Chen, W.; Liu, L.; Liang, X.; Chen, C.; Wang, X.; Peng, Q.; Li, Y. A Versatile Bottom-up Assembly Approach to Colloidal Spheres from Nanocrystals. *Angew. Chem., Int. Ed.* **2007**, *46*, 6650–6653.

31 Wang, G.; Peng, Q.; Li, Y. Upconversion Luminescence of Monodisperse CaF_2:Yb^{3+}/Er^{3+} Nanocrystals. *J. Am. Chem. Soc.* **2009**, *131*, 14200–14201.

32 Huo, Z.; Chen, C.; Chu, D.; Li, H.; Li, Y. Systematic Synthesis of Lanthanide Phosphate Nanocrystals. *Chem.—Eur. J.* **2007**, *13*, 7708–7714.

33 Wang, L.; Li, Y. Controlled Synthesis and Luminescence of Lanthanide Doped $NaYF_4$ Nanocrystals. *Chem. Mater.* **2007**, *19*, 727–734.

34 Wang, G.; Peng, Q.; Li, Y. Luminescence Tuning of Upconversion Nanocrystals. *Chem.—Eur. J.* **2010**, *16*, 4923–4931.

35 Li, P.; Peng, Q.; Li, Y. Dual-Mode Luminescent Colloidal Spheres from Monodisperse Rare-Earth Fluoride Nanocrystals. *Adv. Mater.* **2009**, *21*, 1945–1948.

36 Li, Z.; Zeng, J.; Li, Y. Solvothermal Route to Synthesize Well-Dispersed YBO_3:Eu Nanocrystals. *Small* **2007**, *3*, 438–443.

37 Xie, T.; Li, S.; Peng, Q.; Li, Y. Monodisperse BaF_2 Nanocrystals: Phases, Size Transitions, and Self-Assembly. *Angew. Chem., Int. Ed.* **2009**, *21*, 202–206.

38 Li, S.; Xie, T.; Peng, Q.; Li, Y. Nucleation and Growth of CeF_3 and $NaCeF_4$ Nanocrystals. *Chem.—Eur. J.* **2009**, *15*, 2512–2517.

39 Xie, T.; Li, S.; Peng, Q.; Li, Y. Nucleation and Growth of BaF_xCl_{2-x} Nanorods. *Angew. Chem., Int. Ed.* **2009**, *48*, 196–200.

40 Liu, J.; Li, Y. Synthesis and Self-Assembly of Luminescent Ln^{3+}-Doped $LaVO_4$ Uniform Nanocrystals. *Adv. Mater.* **2007**, *19*, 1118–1122.

41 Wang, X.; Zhuang, J.; Peng, Q.; Li, Y. Hydrothermal Synthesis of Rare-Earth Fluoride Nanocrystals. *Inorg. Chem.* **2006**, *45*, 6661–6665.

42 Wang, L.; Li, Y. $Na(Y_{1.5}Na_{0.5})F_6$ Single-Crystal Nanorods as Multicolor Luminescent Materials. *Nano Lett.* **2006**, *6*, 1645–1649.

43 Huo, Z.; Chen., C.; Li, Y. Self-Assembly of Uniform Hexagonal Yttrium Phosphate Nanocrystals. *Chem. Commun.* **2006**, 3522–3524.

44 Liang, X.; Wang, X.; Zhuang, J.; Peng, Q.; Li, Y. Synthesis of $NaYF_4$ Nanocrystals with Predictable Phase and Shape. *Adv. Mater.* **2007**, *17*, 2757–2765.

45 Liu, J.; Li, Y. General Synthesis of Colloidal Rare Earth Orthovanadate Nanocrystals. *J. Mater. Chem.* **2007**, *17*, 1797–1803.

46 Liang, X.; Wang, X.; Wang, L.; Yan, R.; Peng, Q.; Li, Y. Synthesis and Characterization of Ternary $NH_4Ln_2F_7$ (Ln = Y, Ho, Er, Tm, Yb, Lu) Nanocages. *Eur. J. Inorg. Chem.* **2006**, 2186–2191.

47 Wang, X.; Li, Y. Synthesis and Characterization of Lanthanide Hydroxide Single-Crystal Nanowires. *Angew. Chem., Int. Ed.* **2002**, *41*, 4790–4793.

48 Wang, X.; Li, Y. Fullerene-Like Rare-Earth Nanoparticles. *Angew. Chem., Int. Ed.* **2003**, *42*, 3497–3500.

49 Liang, X.; Wang, X.; Zhuang, J.; Peng, Q.; Li, Y. Branched $NaYF_4$ Nanocrystals with Luminescent Properties. *Inorg. Chem.* **2007**, *46*, 6050–6055.

50 Li, W.; Wang, X.; Li, Y. Single-Step in Situ Synthesis of Double Bond-Grafted Yttrium-Hydroxide Nanotube Core-Shell Structures. *Chem. Commun.* **2004**, 164–165.

51 Wang, X.; Li, Y. Rare-Earth-Compound Nanowires, Nanotubes, and Fullerene-Like Nanoparticles: Synthesis, Characterization, and Properties. *Chem.—Eur. J.* **2003**, *9*, 5627–5635.

52 Ge, J.; Chen, W.; Liu, L.; Li, Y. Formation of Disperse Nanoparticles at the Oil/Water Interface in Normal Microemulsions. *Chem.—Eur. J.* **2006**, *12*, 6552–6558.

53 Sun, X.; Liu, J.; Li, Y. Use of Carbonaceous Polysaccharide Microspheres as Templates for Fabricating Metal Oxide Hollow Spheres. *Chem.—Eur. J.* **2006**, *12*, 2039–2047.

54 Li, Y.; Huang, Y.; Bai, T.; Li, L. Straightforward Conversion Route to Nanocrystalline Monothiooxides of Rare Earths through a High-Temperature Colloid Technique. *Inorg. Chem.* **2000**, *39*, 3418–3420.

55 Zeng, J.; Xie, T.; Li, Z.; Li, Y. Monodispersed Nanocrystalline Fluoroperovskite Up-Conversion Phosphors. *Cryst. Growth Des.* **2007**, *7*, 2774–2777.

56 Zeng, J.; Li, Z.; Su, J.; Wang, L.; Yan, R.; Li, Y. Synthesis of Complex Rare Earth Fluoride Nanocrystal Phosphors. *Nanotechnology* **2006**, *17*, 3549–3555.

57 Sun, X.; Li, Y. Size-Controllable Luminescent Single Crystal CaF_2 Nanocubes. *Chem. Commun.* **2003**, 1768–1769.

58 Liang, X.; Wang, W.; Zhuang, Y.; Xu, B.; Kuang, S.; Li, Y. Formation of CeO_2-ZrO_2 Solid Solution Nanocages with Controllable Structures via Kirkendall Effect. *J. Am. Chem. Soc.* **2008**, *130*, 2736–2737.

59 Yan, R.; Sun, X.; Wang, X.; Peng, Q.; Li, Y. Crystal Structures, Anisotropic Growth, and Optical Properties: Controlled Synthesis of Lanthanide Orthophosphate One-Dimensional Nanomaterials. *Chem.—Eur. J.* **2005**, *11*, 2183–2195.

60 Yan, R.; Li, Y. Down/Up Conversion in Ln^{3+}-Doped YF_3 Nanocrystals. *Adv. Funct. Mater.* **2005**, *15*, 763–770.

61 Lu, Z.; Tang, Y.; Chen, L.; Li, Y. Shape-Controlled Synthesis and Characterization of $BaZrO_3$ Microcrystals. *J. Cryst. Growth* **2004**, *266*, 539–544.

62 Li, Z.; Zeng, J.; Chen, C.; Li, Y. Hydrothermal Synthesis and Luminescent Properties of YBO_3:Tb^{3+} Uniform Ultrafine Phosphor. *J. Cryst. Growth* **2006**, *286*, 487–493.

63 Wang, X.; Sun, X.; Yu, D.; Zou, B.; Li, Y. Rare Earth Compound Nanotubes. *Adv. Mater.* **2003**, *15*, 1442–1445.

64 Zeng, J.; Su, J.; Li, Z.; Yan, R.; Li, Y. Synthesis and Upconversion Luminescence of Hexagonal-Phase $NaYF_4$:Yb, Er^{3+} Phosphors of Controlled Size and Morphology. *Adv. Mater.* **2005**, *17*, 2119–2123.

65 Wang, D.; Wang, Z.; Zhao, P.; Zheng, W.; Peng, Q.; Liu, L.; Chen, X.; Li, Y. Rare-Earth Oxide Nanostructures: Rules of Rare-Earth Nitrate Thermolysis in ODA. *Chem.—Asian J.* **2010**, *5*, 925–931.

66 Liu, J.; Yao, Q.; Li, Y. Effects of Downconversion Luminescent Film in Dye-Sensitized Solar Cells. *Appl. Phys. Lett.* **2006**, *88*, No. 173119.

67 Liang, X.; Wang, X.; Zhuang, J.; Chen, Y.; Wang, D.; Li, Y. Synthesis of Nearly Monodisperse Iron Oxide and Oxyhydroxide Nanocrystals. *Adv. Funct. Mater.* **2006**, *16*, 1805–1813.

68 Wang, L.; Li, Y. Luminescent Nanocrystals for Nonenzymatic Glucose Concentration Determination. *Chem.—Eur. J.* **2007**, *13*, 4203–4207.

69 Wang, L.; Li, Y. Green Upconversion Nanocrystals for DNA Detection. *Chem. Commun.* **2006**, 2557–2559.

70 Yao, Q.; Liu, J.; Peng, Q.; Wang, X.; Li, Y. Nd-Doped TiO_2 Nanorods: Preparation and Application in Dye-Sensitized Solar Cells. *Chem.—Asian J.* **2006**, *1*, 737–741.

71 Wang, D.; Xie, T.; Li, Y. Nanocrystals: Solution-Based Synthesis and Applications as Nanocatalysts. *Nano Res.* **2009**, *2*, 30–46.

72 Zhou, K.; Wang, X.; Sun, X.; Peng, Q.; Li, Y. Enhanced Catalytic Activity of Ceria Nanorods from Well-Defined Reactive Crystal Planes. *J. Catal.* **2005**, *229*, 206–212.

73 Wang, X.; Li, Y. Monodisperse Nanocrystals: General Synthesis, Assembly, and Their Applications. *Chem. Commun.* **2007**, 2901–2910.

74 Wang, L.; Yan, R.; Huo, Z.; Wang, L.; Zeng, J.; Bao, J.; Wang, X.; Peng, Q.; Li, Y. Fluorescence Resonant Energy Transfer Biosensor Based on Upconversion-Luminescent Nanoparticles. *Angew. Chem., Int. Ed.* **2005**, *44*, 6054–6057.

75 Yang, Z.; Woo, T.; Hermansson, K. Strong and Weak Adsorption of CO on CeO_2 Surfaces from First Principles Calculations. *Chem. Phys. Lett.* **2004**, *396*, 384–392.

76 Schlögl, R.; Abd Hamid, S. B. Nanocatalysis: Mature Science Revisited or Something Really New? *Angew. Chem., Int. Ed.* **2004**, *43*, 1628–1637.

77 Chrzanowski, W.; Wiechkowski, A. Surface Structure Effects in Platinum/Ruthenium Methanol Oxidation Electrocatalysis. *Langnuir* **1998**, *14*, 1967–1970.

78 Choudary, B. M.; Mulukutla, R. S.; Klabunde, K. J. Benzylation of Aromatic Compounds with Different Crystallites of MgO. *J. Am. Chem. Soc.* **2003**, *125*, 2020–2021.